

C: Energy Conversion and Storage; Energy and Charge Transport

Order-Disorder Transition in Kesterite CuZnSnS: Thermopower Enhancement via Electronic Band Structure Modification

Eleonora Isotta, Binayak Mukherjee, Carlo Fanciulli, Nicola Maria Pugno, and Paolo Scardi

J. Phys. Chem. C, **Just Accepted Manuscript** • DOI: 10.1021/acs.jpcc.0c00886 • Publication Date (Web): 09 Mar 2020

Downloaded from pubs.acs.org on March 18, 2020

Just Accepted

"Just Accepted" manuscripts have been peer-reviewed and accepted for publication. They are posted online prior to technical editing, formatting for publication and author proofing. The American Chemical Society provides "Just Accepted" as a service to the research community to expedite the dissemination of scientific material as soon as possible after acceptance. "Just Accepted" manuscripts appear in full in PDF format accompanied by an HTML abstract. "Just Accepted" manuscripts have been fully peer reviewed, but should not be considered the official version of record. They are citable by the Digital Object Identifier (DOI®). "Just Accepted" is an optional service offered to authors. Therefore, the "Just Accepted" Web site may not include all articles that will be published in the journal. After a manuscript is technically edited and formatted, it will be removed from the "Just Accepted" Web site and published as an ASAP article. Note that technical editing may introduce minor changes to the manuscript text and/or graphics which could affect content, and all legal disclaimers and ethical guidelines that apply to the journal pertain. ACS cannot be held responsible for errors or consequences arising from the use of information contained in these "Just Accepted" manuscripts.

Order-Disorder Transition in Kesterite $\text{Cu}_2\text{ZnSnS}_4$: Thermopower Enhancement via Electronic Band Structure Modification

*Eleonora Isotta,^{a,b} Binayak Mukherjee,^a Carlo Fanciulli,^c Nicola M. Pugno,^{a,b,d,e} and Paolo Scardi^{*a}*

^a Department of Civil, Environmental and Mechanical Engineering, University of Trento, via Mesiano 77, 38123 Trento, Italy

^b Laboratory of Bio-inspired, Bionic, Nano, Meta Materials & Mechanics, Department of Civil, Environmental and Mechanical Engineering, University of Trento, via Mesiano 77, 38123 Trento, Italy

^c National Research Council of Italy-Institute of Condensed Matter Chemistry and Technologies for Energy (CNR-ICMATE), Lecco Unit, via Previati 1/E, 23900 Lecco, Italy

^d Ket-Lab, Edoardo Amaldi Foundation, Via del Politecnico snc, 00133 Rome, Italy

^e School of Engineering and Materials Science, Queen Mary University of London, Mile End Road, London E1 4NS, UK

ABSTRACT

The order-disorder transition of kesterite (CZTS, $\text{Cu}_2\text{ZnSnS}_4$) from $I-4$ to $I-42m$ crystal structures has a marked effect on Seebeck coefficient, which displays a sharp enhancement at the transition temperature, around 533K. Considered to be detrimental for the performance of photovoltaic kesterite, the order-disorder transition appears to be beneficial for thermopower. Experimental data and *ab initio* calculations explain the origin of this enhancement: the increase of crystal symmetry in the disordered polymorph leads to a favorable electronic band structure characterized by flat and converged bands. At the transition, a sharp drop in mobility and increase in carrier concentration experimentally prove this mechanism of Seebeck enhancement. This, other than providing a new understanding of the material, can cast light on some profitable mechanisms to enhance the thermoelectric performance. Additionally, the increase in Seebeck provides an efficient tool to observe the transition and possibly to quantify disorder.

1. Introduction

Kesterite (CZTS) is a p-type chalcogenide material with reference formula $\text{Cu}_2\text{ZnSnS}_4$. It has long been studied as absorber in thin film photovoltaic devices,¹⁻³ and recently deemed promising as a potential thermoelectric material,⁴⁻¹⁰ valued for its intrinsically low thermal conductivity⁴ and composition based on non-toxic, abundant and low-cost elements.¹¹ In its ordered and low temperature form, kesterite is reported having a tetragonal $I-4$ crystal structure, while it was recently proved that a cubic $F-43m$ low-temperature polymorph can be obtained for samples made by high-energy ball-milling, as an effect of a high disorder state of the cations.^{4,12} This appears to be a metastable phase, since it transitions to the tetragonal polymorph on heating, as the temperature activates a reordering of the cations.⁴ At around 533K, tetragonal kesterite faces a reversible order-disorder phase transition: cations in the intermediate Cu-Zn planes of the $I-4$ structure ($2c$ and $2d$ Wyckoff positions) completely randomize their position (becoming $4d$ Wyckoff position) thus transitioning to the tetragonal $I-42m$ structure.^{5,13-15} This transition has been studied in some detail in recent years, because disorder is considered detrimental for the photovoltaic performance of CZTS, as well as difficult to avoid. In fact, owing to the low formation energy of the Cu_{Zn} and Zn_{Cu} antisite defects,^{16,17} a certain degree of disorder is inevitable in CZTS, even after extensive annealing treatments. Significant efforts have been made to quantify the degree of disorder and the subsequent loss in photovoltaic efficiency, rarely finding an ultimately suitable technique.^{5,14} Nevertheless, for what concerns thermoelectric performance things proved to be different: the order-disorder transition has a marked and beneficial effect on the Seebeck coefficient.⁵

The aim of this work is to demonstrate experimentally and through *ab initio* calculations the physical origin of the increase in thermopower caused by the order-disorder transition of kesterite, which we connect with the crystal-symmetry induced modification of the electronic band structure. We also show how the degree of order of a sample affects the Seebeck coefficient.

2. Methods

2.1 Experimental

Bulk kesterite sintered disks were produced according to previously described procedures,^{4,5} starting from reactive ball milling of the elementary components, i.e., metals and sulfur in stoichiometric proportions, to obtain kesterite nanometric powders, then cold-pressed and thermally treated. Some of the samples undergone a quenching process in air, either starting from the sintering temperature of 560°C, or from a lower temperature reached with natural cooling, to room temperature. Absolute Seebeck coefficient measurements have been performed in 4-contact configuration and with Pt standard with a Linseis LZT Meter, in the temperature range 320K-720K, with a temperature gradient of 10K. Carrier density and mobility have been measured with an MMR K-20 and an H-50 measurement systems. Results are obtained by a combined measurement of Hall effect and resistivity as a function of temperature. Resistivity is determined by the Van Der Pauw method using squared shaped samples with thickness below 1 mm, providing an optimal geometrical ratio between surface and thickness. Hall effect measurements have been performed with a permanent-magnet field of 6270±10 G. The currents for testing have been set to values below 10 mA in order to prevent any thermal change in the samples. All the measurements are performed in vacuum, to prevent material degradation, and in the temperature range 300K-620K.

2.2 Density Functional Theory (DFT) calculations

The ab initio electronic structure calculations with DFT have been performed using the plane wave basis set implemented in the Vienna ab initio simulation package (VASP).^{18,19} The electron-exchange correlation functional was approximated using the Perdew-Burke-Ernzerhof (PBE)²⁰ form of the generalized gradient approximation (GGA). All calculations were performed with an energy cut-off of 300 eV. The ordered and disordered structures were modelled with 16 and 64 atom supercells respectively, visible in Figure 1, and the geometry was optimized with an 8x8x8 and 4x4x4 Monkhorst Pack (MP) k-mesh, respectively, centered at the Γ point, with Gaussian charge smearing in the order of 0.01 eV. The electronic degrees of freedom were relaxed until the change in the total free energy and energy eigenvalues were both smaller than 10^{-6} eV. The disordered structure was generated by manually assigning a random Cu/Zn arrangement in the $4d$ Wyckoff positions of the $I-42m$ structure, keeping the overall stoichiometry balanced (Cu:Zn = 1:1 in $4d$ sites). The bands were calculated along a high-symmetry path in the irreducible Brillouin zone obtained using the SeeK-path²¹ tool, while the electronic density of states (*DoS*) was obtained using a dense 24x24x24 MP k-mesh for the 16-atom supercell and an 8x8x8 MP k-mesh for the 64-atom supercells.

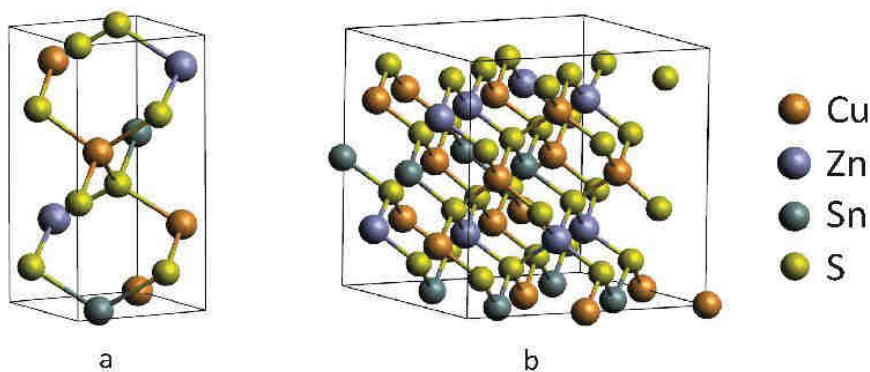


Figure 1. Supercell crystal structures of kesterite used in DFT calculations: (a) ordered, s.g. $I-4$ and 16-atom cell; (b) disordered, s.g. $I-42m$ and 64-atom supercell.

3. Results and discussion

3.1 Thermoelectric properties

The order-disorder phase transition of kesterite, from the ordered $I-4$ to the disordered $I-42m$ tetragonal structures, has been reported at $533\text{K} \pm 10\text{K}$.^{13,14} As shown by thermal analyses, it is a second-order and reversible transition,⁵ and it consists of a full occupational disorder of Cu and Zn cations in the $4d$ Wyckoff positions. This transition appears to have a beneficial role for thermoelectric CZTS. Indeed, the measurement of Seebeck coefficient, reproduced in Figure 2a, displays a sharp increase around the transition temperature.⁵ Insets of Figure 2a show the ordered $I-4$ crystal structure for the region below the transition temperature, where Cu and Zn occupy specific positions in the intermediate planes, and the disordered $I-42m$ structure for the high-temperature region, where a unique position is considered to account for a mixed and random occupation of the two cations. We have put forward that this enhancement is due to a higher symmetry in the crystal structure of disordered CZTS.⁵ Indeed, due to this loss of specificity in the positions of Cu and Zn, the disordered is a more symmetric structure. This can also be noticed by the additional 2-fold rotation axis and mirror plane specified in the space group $I-42m$.

Figure 2b shows the electrical resistivity measured in Van Der Pauw configuration, while Figure 2c displays the carrier concentration, measured via Hall effect on the same sample, and the carrier mobility, calculated from resistivity and carrier concentration data. Around

the order-disorder transition temperature we notice a substantial increase in carrier concentration, that nearly triples its values, and a corresponding decrease in mobility. We observe a kink in resistivity (Figure 2b) around the transition temperature. It is worth mentioning that literature data reports a smaller electronic bandgap E_g for disordered kesterite (~ 1.50 eV) with respect to ordered (~ 1.67 eV).^{15,22}

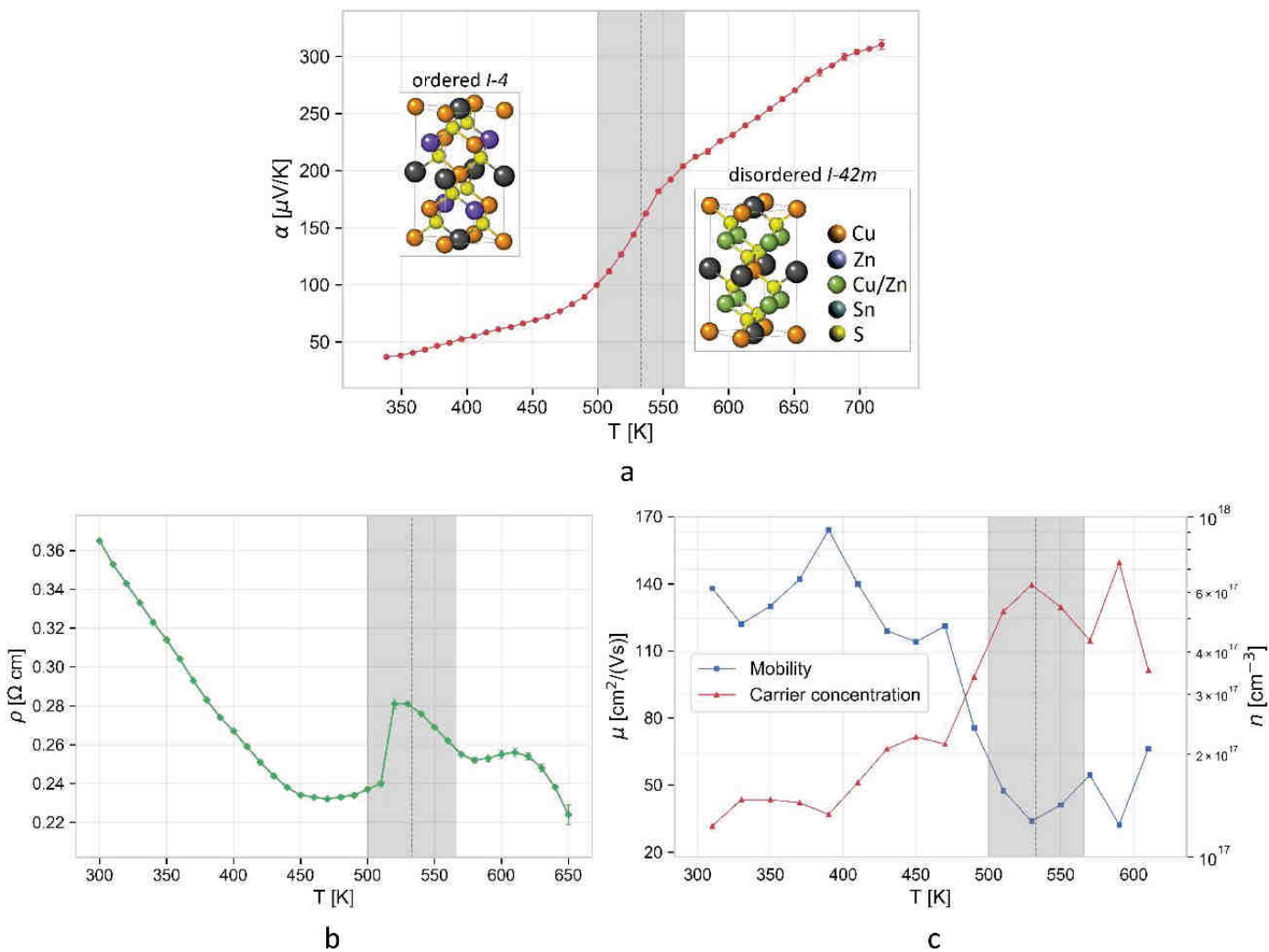


Figure 2. (a) Absolute Seebeck coefficient α (standard deviation is expressed with error bars) with insets showing the relevant kesterite crystal structures for each temperature region, namely ordered $I-4$ in the low-temperature and disordered $I-42m$ in the high-temperature zone. Data reproduced from Ref.⁵ with permission from MDPI. (b) Electrical resistivity ρ (standard deviation is expressed with error bars), (c) and carrier mobility μ and concentration n (in logarithmic scale) measured for a bulk CZTS sample. In the order-disorder transition region (highlighted in grey) it is possible to notice an increase in Seebeck coefficient and carrier concentration, and a corresponding drop in the mobility. This is attributed to band structure modifications: crystal-symmetry induced band convergence and reduction of curvature.

3.2 Electronic band structure

In order to provide a theoretical explanation for the experimentally observed changes in thermopower, electrical resistivity, carrier mobility and carrier concentration caused by the order-disorder transition, we performed *ab initio* band structure calculations for ordered (Figure 3a) and disordered (Figure 3b) kesterite. From these calculations we observe a threefold effect on the bands caused by the transition from the ordered to the disordered phase. Firstly, we see an increased convergence at the top of the valence band in the disordered phase, with the separation between the top three bands dropping from 0.139 eV (~ 5.51 kT, calculated at $T = 298$ K) for the ordered phase to 0.072 eV (~ 1.39 kT, calculated at $T = 600$ K) for the disordered. Secondly, we observe a significant reduction in curvature (flattening) at the top of the valence band in the disordered phase compared to the ordered. Finally, we observe a decrease in the band gap going from the ordered to the disordered phase, though it must be considered that the exchange-correlation functional in GGA is known to strongly underestimate the band gap. While more sophisticated calculations using hybrid functionals do provide a better estimation of the band gap, they become prohibitively expensive in terms of computational resources, particularly for larger supercells such as the disordered structures. It may be assumed that the errors for similar systems are similar and cancel out in comparative studies, the accuracy of the calculations being validated by their agreement with experiments. The effect of an increased band convergence and a reduced curvature due to higher disorder in the crystal structure is evidenced also by the density of states (*DoS*), presented in Figure 3c, which is higher at the top of the valence band, with steeper slope of *DoS* (and of

$\ln(DoS)$, in the inset) for the disordered phase with respect to the ordered. The asymmetry of the DoS with respect to the Fermi level is consistent with the p character of the material. In the Supporting Information, the extended band structures are visible, as well as the band structures for a partially disordered sample and another configuration of disorder, to confirm and generalize the validity of the DFT results.

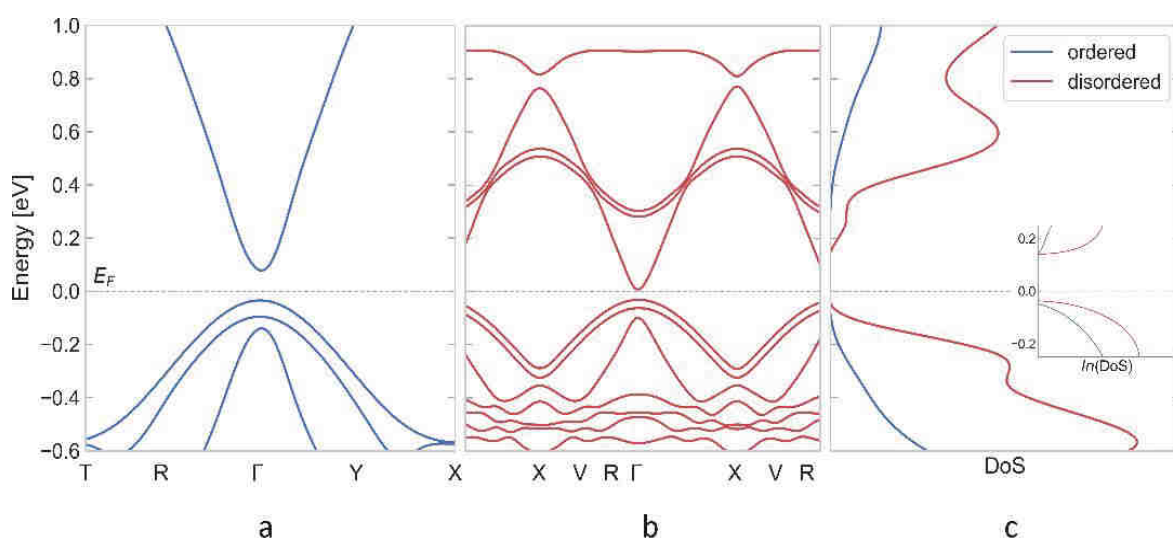


Figure 3. Band structures for ordered (a), and disordered (b) kesterite. Panel (c) displays the density of states DoS , with inset showing the natural logarithm of the DoS . With an increase of disorder, the top valence bands tend to converge and reduce their curvature, the bandgap narrows, while DoS and $\ln(DoS)$ get higher and steeper. We believe this band structure modification is at the origin of the difference in electrical properties. The Fermi energy is set to 0 eV in each case. X-axis is on the same scale in k-space for (a) and (b).

3.3 Order-disorder transition: crystal symmetry induces band convergence and flatness

The thermopower is directly proportional to the density of state effective mass $m_{DoS}^* = N_V^{2/3} m_I^*$, where N_V is the band degeneracy and m_I^* is the inertial effective mass of charge carriers along the conduction direction.²³ It has been pointed out in the literature that there may be a connection between an increase in the symmetry of a crystal structure and an

improved band convergence.^{24–26} We believe the order-disorder transition of CZTS to be an example of this behavior: the higher crystal symmetry causes an increase in the electronic band degeneracy N_V , as proved by DFT, thus justifying the sharp growth in the experimentally observed Seebeck coefficient. We attribute the observed increase in carrier concentration (Figure 2b) both to the decrease in E_g and to the convergence of bands. In fact, were it due to a narrower bandgap alone, we would expect a corresponding decrease in thermopower and electrical resistivity, while experimental data shows that thermopower increases with the transition whereas resistivity does not decrease. A higher band convergence could instead explain why we observe an enhancement of Seebeck despite the increase in carrier concentration. Resistivity displays a sharp upwards kink around the transition temperature, and then smoothly decreases to reach values in the order of those obtained prior to the transition. This is also in contradiction with the increased carrier concentration and can only be explained with the observed sharp drop in mobility, which in this case we associate to a carrier localization due to band convergence. In many literature cases, a pronounced decrease in mobility is associated to an enhancement of thermopower,²⁷ along with a steeper DoS as expressed by Mott's formula.²⁸ Moreover, from *ab initio* calculations we observe a reduced curvature in the valence bands, which is in agreement with an increased m_l^* and decreased mobility. Indeed, the movement of cations and the concurring rearrangement of covalent bonds happening during the transition might have promoted a higher number of available energy levels (therefore higher carrier concentration) but more localized (causing the drop in mobility and the increase in Seebeck). This, contrary to what reported for other systems,^{29,30} seems to not extensively penalize electrical resistivity owing to the

simultaneous increase in carrier concentration caused by band convergence. The DoS , being higher for the disordered phase, highlights the higher availability of valence states close to the Fermi level and their higher occupation, associated to the reduced bandgap. The trend of the logarithm of the density of states (shown in the inset of Figure 3c) is steeper at the top of the valence band for the disordered polymorph, in agreement with the higher thermopower provided for by Mott's formula.²⁸ Furthermore, a sharper asymmetry of the DoS with respect to the Fermi level is found which is consistent with the p-type nature and is typically associated with an increase in Seebeck.²⁸ In general, the DFT calculations are in good agreement with the experimental results. It is evident that the described phenomenon is dominated by band features (flatness and degeneracy), which is also supported by the low value of carrier concentration (in the order of 10^{17} cm^{-3}) and can explain why we observe a decoupling of the thermopower and resistivity trends. These results provide experimental and theoretical proof that favorable band structure and the subsequent enhancement of thermoelectric properties can be achieved with an increase in crystal symmetry.

3.4 Seebeck as a method to observe the transition and estimate the degree of order

In the photovoltaic community, much research has been performed on methods to determine the degree of order in kesterite samples, as the lower bandgap of the disordered phase is deemed responsible for open-circuit voltage losses, thus undermining the solar-cell efficiency.¹³ However, the search for a suitable and convenient technique, able to observe a clear difference between samples with different degrees of order, has proved a complex challenge. In fact, X-ray diffraction is not suitable for observing Cu-Zn disorder, because Cu^+ and Zn^{2+} are isoelectronic and appear identical to X-rays. Other proposed

1
2
3 methods include Raman spectroscopy, through the quantification of the relative intensity
4 of secondary peaks,^{13,14,31,32} optical measurements,^{15,22} solid-state nuclear magnetic
5 resonance³³ and neutron scattering³⁴. In this context, we tentatively propose the Seebeck
6 measurement as an alternative technique, as it proves efficient in observing the Cu-Zn
7 transition of kesterite and sensitive to the degree of order in the sample. Indeed, we have
8 experimentally observed that according to the level of order in the crystal structure at the
9 beginning of the measurement, the transition appears in a different way. Figure 4 shows
10 the trends of Seebeck coefficient for some of our CZTS samples characterized by
11 different thermal histories, which is known to influence the degree of order.^{13,14} Sample 1
12 has been obtained by quenching right after the sintering process, at 560°C. This has been
13 done to quench the fully disordered state of the crystal structure, and indeed the sample,
14 on following heating, exhibits a flat trend of Seebeck coefficient, proving that no
15 transition occurs.⁵ A second measurement was then performed on the same sample after
16 letting it to slowly cool down to ambient temperature (water cooling, ~ 2 h long). Sample
17 2 has instead been obtained by allowing it to naturally cool down to 450°C after the
18 thermal treatment, and then suddenly quenched to room temperature. The measurement of
19 Seebeck coefficient displays a small increase around the transition temperature, pointing
20 out that the sample was in a partly disordered state. These measurements point out that
21 the degree of order can influence the behavior of Seebeck coefficient. Several research
22 groups working on thermoelectric CZTS have reported different trends for Seebeck: some
23 of them present a flat curve, that apparently does not display the order-disorder
24 transition;^{6,7} Sharma *et al.*, instead, report trends where an increase is visible around the
25 transition temperature.^{9,10} Based on the present results, the reason for this inconsistency of
26
27
28
29
30
31
32
33
34
35
36
37
38
39
40
41
42
43
44
45
46
47
48
49
50
51
52
53
54
55
56
57
58
59
60

experimental results can be ascribed to different degree of order, as samples from the literature have diverse production routes and thermal histories, therefore being different in terms of ordering kinetics. Moreover, the band structure for a partially disordered sample, shown in Figure S3a of the Supporting Information, exhibits an intermediate behavior with respect to the ordered and fully disordered one, with a closer similarity to the latter. This is consistent with the definition of random occupation of Cu and Zn cations for the disordered structure, which will also include some narrow regions of order.

Nevertheless, this dependence could be exploited to retrieve information on the sample, here just qualitatively illustrated. Through a suitable empirical calibration with other techniques or a suitable theoretical model, thermopower could be used to retrieve an order parameter and to estimate the degree of order in a sample.

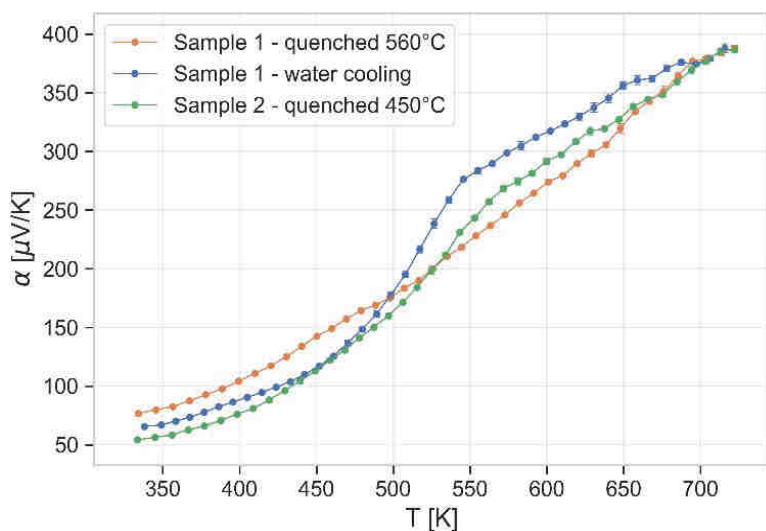


Figure 4. Absolute Seebeck coefficient α for some CZTS samples: quenched from 560°C to preserve the disordered state, for the same sample after water cooling, and for a second sample, characterized by an intermediate disorder state.

4. Conclusions

The order-disorder transition of kesterite from ordered $I-4$ to disordered $I-42m$ crystal structures leads to a beneficial effect on thermopower that presents an increase around the transition temperature of 533K,⁵ conversely to what happens for photovoltaic kesterite for which the transition is deemed detrimental for the performance.¹⁴ In this work, we have demonstrated that the mechanism at the origin of this enhancement of Seebeck coefficient is an improved electronic band structure. DFT calculations show more converged and flatter bands for the disordered polymorph, which lead to an increased carrier concentration and a decreased mobility, confirmed by experimental data. A higher crystal symmetry for the disordered structure is deemed responsible for the improved band degeneracy, which in turn leads to a higher density of states effective mass and enhanced thermopower. Electrical resistivity, differently from what commonly occurs,^{29,30} is not penalized by the low mobility due to the concurrent high carrier concentration originated from band convergence. These results, besides providing a new understanding of the studied material, can cast light on some profitable mechanisms to enhance the thermoelectric performance. Additionally, the measurement of Seebeck coefficient proved to be a simple and efficient way to observe the order-disorder transition of kesterite; as shown in this work, a different degree of order in the crystal structure causes the increase of Seebeck at the order-disorder transition to vary. This dependence could be exploited to estimate the degree of order in a sample, which has always been considered difficult to attribute due to the low sensitivity of other proposed methods.^{13,33} Furthermore, it could explain the difference found in the literature for CZTS in the trends of Seebeck coefficient, especially where the order-disorder transition is not explicitly observed or identified.^{6,7,9,10}

ASSOCIATED CONTENT

Supporting Information. Additional DFT calculations for other configurations of disordered kesterite (PDF).

AUTHOR INFORMATION

Corresponding Author

*Email: paolo.scardi@unitn.it; Tel: +39 0461 282417; Address: 38123 via Mesiano 77, Trento, Italy

Author Contributions

The manuscript was written through contributions of all authors. All authors have given approval to the final version of the manuscript.

ACKNOWLEDGMENT

This research was funded by the Autonomous Province of Trento, within the framework of the programmatic Energy Action 2015–2017. The computational time was provided by CINECA - Italian Supercomputing Facility, with the project CZTS - HP10CONX70.

N.M.P. is supported by the European Commission under the Graphene Flagship Core 2 grant No. 785219 (WP14, “Composites”), the FET Proactive (“Neurofibres”) grant No. 732344, the FET Open (Boheme) grant No. 863179 as well as by the Italian Ministry of Education, University and Research (MIUR) under the “Departments of Excellence” grant L. 232/2016, the ARS01- 01384-PROSCAN and the PRIN-20177TTP3S grants.

REFERENCES

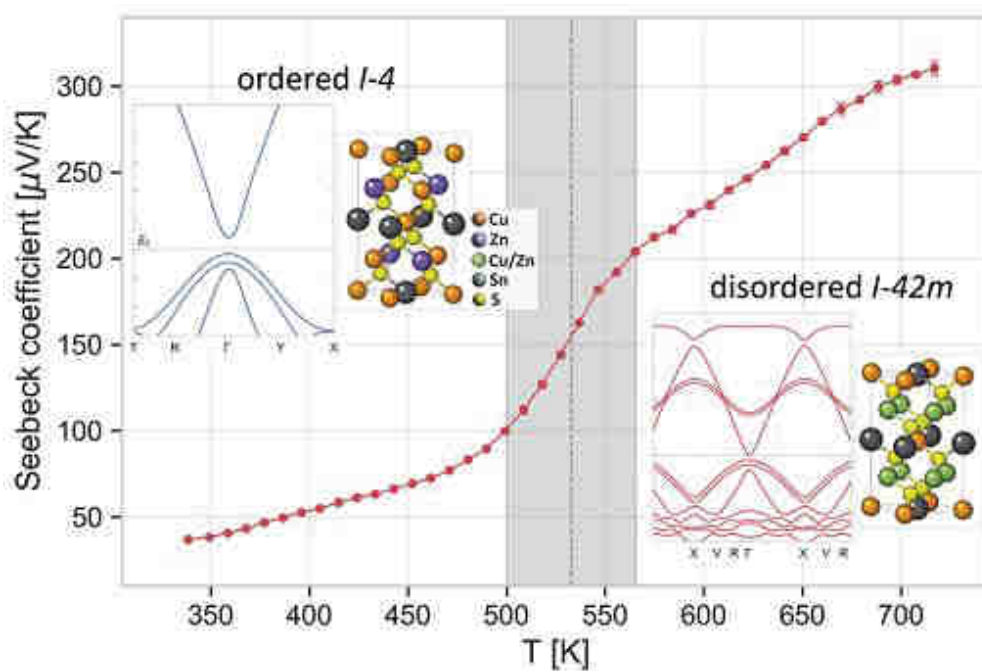
- (1) Katagiri, H.; Jimbo, K.; Yamada, S.; Kamimura, T.; Maw, W. S.; Fukano, T.; Ito, T.; Motohiro, T. Enhanced Conversion Efficiencies of Cu₂ZnSnS₄-Based Thin Film Solar Cells by Using Preferential Etching Technique. *Appl. Phys. Express* **2008**, *1* (4), 0412011–0412012. <https://doi.org/10.1143/APEX.1.041201>.
- (2) Ataollahi, N.; Malerba, C.; Ciancio, R.; Edla, R.; Scardi, P.; Cappelletto, E.; Di Maggio, R. Control of Composition and Grain Growth in Cu₂ZnSnS₄ Thin Films from Nanoparticle Inks. *Thin Solid Films* **2019**, *674*, 12–21. <https://doi.org/10.1016/j.tsf.2019.02.004>.
- (3) Syafiq, U.; Ataollahi, N.; Maggio, R. Di; Scardi, P. Solution-Based Synthesis and Characterization of Cu₂ZnSnS₄ (CZTS) Thin Films. *Molecules* **2019**, *24* (19), 3454. <https://doi.org/10.3390/molecules24193454>.
- (4) Isotta, E.; Pugno, N. M.; Scardi, P. Nanostructured Kesterite (Cu₂ZnSnS₄) for Applications in Thermoelectric Devices. *Powder Diffr.* **2019**, *0* (0), 2–7. <https://doi.org/10.1017/S0885715619000277>.
- (5) Isotta, E.; Fanciulli, C.; Pugno, N. M.; Scardi, P. Effect of the Order-Disorder Transition on the Seebeck Coefficient of Nanostructured Thermoelectric Cu₂ZnSnS₄. *Nanomaterials* **2019**, *9* (5), 762. <https://doi.org/10.3390/nano9050762>.
- (6) Liu, M. L.; Huang, F. Q.; Chen, L. D.; Chen, I. W. A Wide-Band-Gap p -Type Thermoelectric Material Based on Quaternary Chalcogenides of Cu₂ZnSnQ₄(Q=S,Se). *Appl. Phys. Lett.* **2009**, *94* (20), 202103. <https://doi.org/10.1063/1.3130718>.
- (7) Yang, H.; Jauregui, L. A.; Zhang, G.; Chen, Y. P.; Wu, Y. Non-Toxic and Abundant Copper Zinc Tin Sulfide Nanocrystals for Potential High Temperature Thermoelectric Energy Harvesting. *Nano Lett.* **2012**. <https://doi.org/10.1021/nl201718z>.
- (8) Kumar, S.; Ansari, M. Z.; Khare, N. Influence of Compactness and Formation of Metallic Secondary Phase on the Thermoelectric Properties of Cu₂ZnSnS₄ Thin Films. *Thin Solid Films* **2018**, *645*, 300–304. <https://doi.org/10.1016/j.tsf.2017.11.001>.
- (9) Sharma, S. D.; Neeleshwar, S. Thermoelectric Properties of Hot Pressed CZTS Micro

- Spheres Synthetized by Microwave Method. *MRS Adv.* **2018**, 3 (24 (Energy and Sustainability)), 1373–1378. <https://doi.org/10.1557/adv.2018>.
- (10) Sharma, S. D.; Khasimsaheb, B.; Chen, Y. Y.; Neeleshwar, S. Enhanced Thermoelectric Performance of $\text{Cu}_2\text{ZnSnS}_4$ (CZTS) by Incorporating Ag Nanoparticles. *Ceram. Int.* **2019**, 45 (2), 2060–2068. <https://doi.org/10.1016/j.ceramint.2018.10.109>.
- (11) Adachi, S. *Earth-Abundant Materials for Solar Cells*; 2015.
- (12) Kapusta, K.; Drygas, M.; Janik, J. F.; Jelen, P.; Bucko, M. M.; Olejniczak, Z. From Magnetic Cubic Pre-Kesterite to Semiconducting Tetragonal Kesterite $\text{Cu}_2\text{ZnSnS}_4$ Nanopowders via the Mechanochemically Assisted Route. *J. Alloys Compd.* **2019**, 770, 981–988. <https://doi.org/10.1016/j.jallcom.2018.08.135>.
- (13) Scragg, J. J. S.; Choubrac, L.; Lafond, A.; Ericson, T.; Platzer-Björkman, C. A Low-Temperature Order-Disorder Transition in $\text{Cu}_2\text{ZnSnS}_4$ Thin Films. *Appl. Phys. Lett.* **2014**, 104 (041911), 041911. <https://doi.org/10.1063/1.4863685>.
- (14) Scragg, J. J. S.; Larsen, J. K.; Kumar, M.; Persson, C.; Sendler, J.; Siebentritt, S. Cu–Zn Disorder and Band Gap Fluctuations in $\text{Cu}_2\text{ZnSn}(\text{S},\text{Se})_4$: Theoretical and Experimental Investigations. *Phys. Status Solidi B* **2016**, 253 (2), 247–254. <https://doi.org/10.1002/pssb.201552530>.
- (15) Valentini, M.; Malerba, C.; Menchini, F.; Tedeschi, D.; Polimeni, A.; Capizzi, M.; Mittiga, A. Effect of the Order-Disorder Transition on the Optical Properties of $\text{Cu}_2\text{ZnSnS}_4$. *Appl. Phys. Lett.* **2016**, 108, 211909. <https://doi.org/10.1063/1.4952973>.
- (16) Chen, S.; Gong, X. G.; Walsh, A.; Wei, S. Defect Physics of the Kesterite Thin-Film Solar Cell Absorber. **2010**, 96, 021902. <https://doi.org/10.1063/1.3275796>.
- (17) Chen, S.; Walsh, A.; Gong, X.; Wei, S. Classification of Lattice Defects in the Kesterite $\text{Cu}_2\text{ZnSnS}_4$ and $\text{Cu}_2\text{ZnSnSe}_4$ Earth-Abundant Solar Cell Absorbers. *Adv. Mater.* **2013**, No. 25, 1522–1539. <https://doi.org/10.1002/adma.201203146>.
- (18) Kresse, G.; Furthmüller, J. Efficient Iterative Schemes for Ab Initio Total-Energy Calculations Using a Plane-Wave Basis Set. *Phys. Rev. B - Condens. Matter Mater. Phys.* **1996**, 54 (16), 11169–11186. <https://doi.org/10.1103/PhysRevB.54.11169>.
- (19) Kresse, G.; Furthmüller, J. Efficiency of Ab-Initio Total Energy Calculations for Metals and Semiconductors Using a Plane-Wave Basis Set. *Comput. Mater. Sci.* **1996**, 6 (1), 15–50. [https://doi.org/10.1016/0927-0256\(96\)00008-0](https://doi.org/10.1016/0927-0256(96)00008-0).

- (20) Perdew, J. P.; Burke, K.; Ernzerhof, M. Generalized Gradient Approximation Made Simple. *Phys. Rev. Lett.* **1996**, *77* (18), 3865–3868. <https://doi.org/10.1103/PhysRevLett.77.3865>.
- (21) Hinuma, Y.; Pizzi, G.; Kumagai, Y.; Oba, F.; Tanaka, I. Band Structure Diagram Paths Based on Crystallography. *Comput. Mater. Sci.* **2017**, *128*, 140–184. <https://doi.org/10.1016/j.commatsci.2016.10.015>.
- (22) Malerba, C.; Valentini, M.; Mittiga, A. Cation Disorder in Cu₂ZnSnS₄ Thin Films : Effect on Solar Cell Performances. *Sol. RRL* **2017**, *1*, 1700101. <https://doi.org/10.1002/solr.201700101>.
- (23) Kittel, C. *Introduction to Solid State Physics-8th Edition*; 2005. <https://doi.org/10.1119/1.1934457>.
- (24) Zeier, W. G.; Zhu, H.; Gibbs, Z. M.; Ceder, G.; Tremel, W.; Snyder, G. J. Band Convergence in the Non-Cubic Chalcopyrite Compounds Cu₂MGeSe₄. *J. Mater. Chem. C* **2014**, *2* (47), 10189–10194. <https://doi.org/10.1039/c4tc02218a>.
- (25) Zeier, W. G. New Tricks for Optimizing Thermoelectric Materials. *Curr. Opin. Green Sustain. Chem.* **2017**, *4*, 23–28. <https://doi.org/10.1016/j.cogsc.2017.02.003>.
- (26) Zhang, Q.; Song, Q.; Wang, X.; Sun, J.; Zhu, Q.; Dahal, K.; Lin, X.; Cao, F.; Zhou, J.; Chen, S.; et al. Deep Defect Level Engineering : A Strategy of Optimizing the Carrier Concentration for High Thermoelectric Performance. *Energy Environ. Sci.* **2018**, *11*, 933–940. <https://doi.org/10.1039/C8ee00112j>.
- (27) Sun, P.; Wei, B.; Zhang, J.; Tomczak, J. M.; Strydom, A. M.; Søndergaard, M.; Iversen, B. B.; Steglich, F. Large Seebeck Effect by Charge-Mobility Engineering. *Nat. Commun.* **2015**, *6* (May), 1–5. <https://doi.org/10.1038/ncomms8475>.
- (28) Mott, N. F.; Jones, H. The Theory of the Properties of Metals and Alloys. *Journal of Chemical Education*. 1936, p 99. <https://doi.org/10.1021/ed014p99>.
- (29) Pei, Y.; Wang, H.; Snyder, G. J. Band Engineering of Thermoelectric Materials. *Adv. Mater.* **2012**, *24* (46), 6125–6135. <https://doi.org/10.1002/adma.201202919>.
- (30) Pei, Y.; Lalonde, A. D.; Wang, H.; Snyder, G. J. Low Effective Mass Leading to High Thermoelectric Performance. *Energy Environ. Sci.* **2012**, *5* (7), 7963–7969. <https://doi.org/10.1039/c2ee21536e>.
- (31) Rudisch, K.; Ren, Y.; Platzer-Bjorkman, C.; Scragg, J. Order-Disorder Transition in B-

Type Cu₂ZnSnS₄ and Limitations of Ordering through Thermal Treatments. *Appl. Phys. Lett.* **2016**, No. 108, 231902. <https://doi.org/10.1063/1.4953349>.

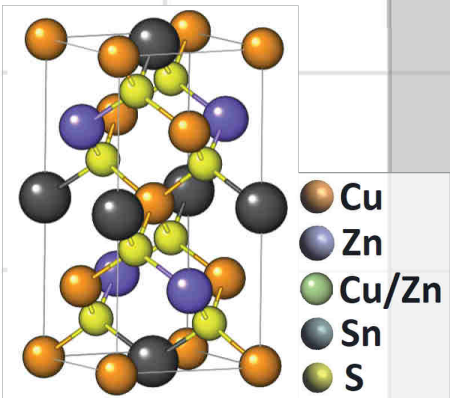
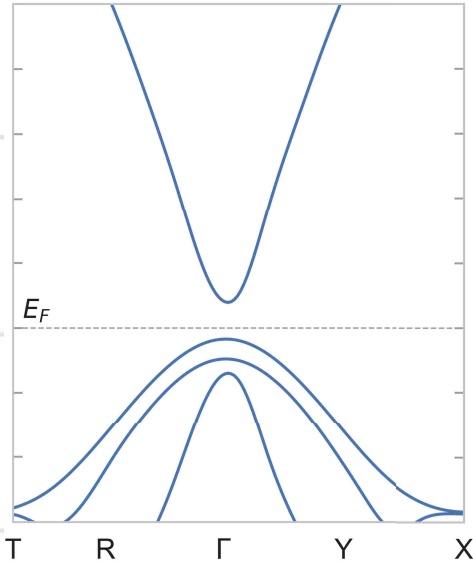
- (32) Rudisch, K.; Davydova, A.; Platzer-björkman, C. The Effect of Stoichiometry on Cu-Zn Ordering Kinetics in Cu₂ZnSnS₄ Thin Films. **2018**, 161558 (October 2017). <https://doi.org/10.1063/1.5010081>.
- (33) Paris, M.; Lafond, A.; Guillot-deudon, C. Solid-State NMR and Raman Spectroscopy To Address the Local Structure of Defects and the Tricky Issue of the Cu/Zn Disorder in Cu-Poor, Zn-Rich CZTS Materials. *Inorg. Chem.* **2014**, 53, 8646–8653. <https://doi.org/10.1021/ic5012346>.
- (34) Ritscher, A.; Hoelzel, M.; Lerch, M. The Order-Disorder Transition in Cu₂ZnSnS₄ – A Neutron Scattering Investigation. *J. Solid State Chem.* **2016**, 238. <https://doi.org/10.1016/j.jssc.2016.03.013>.



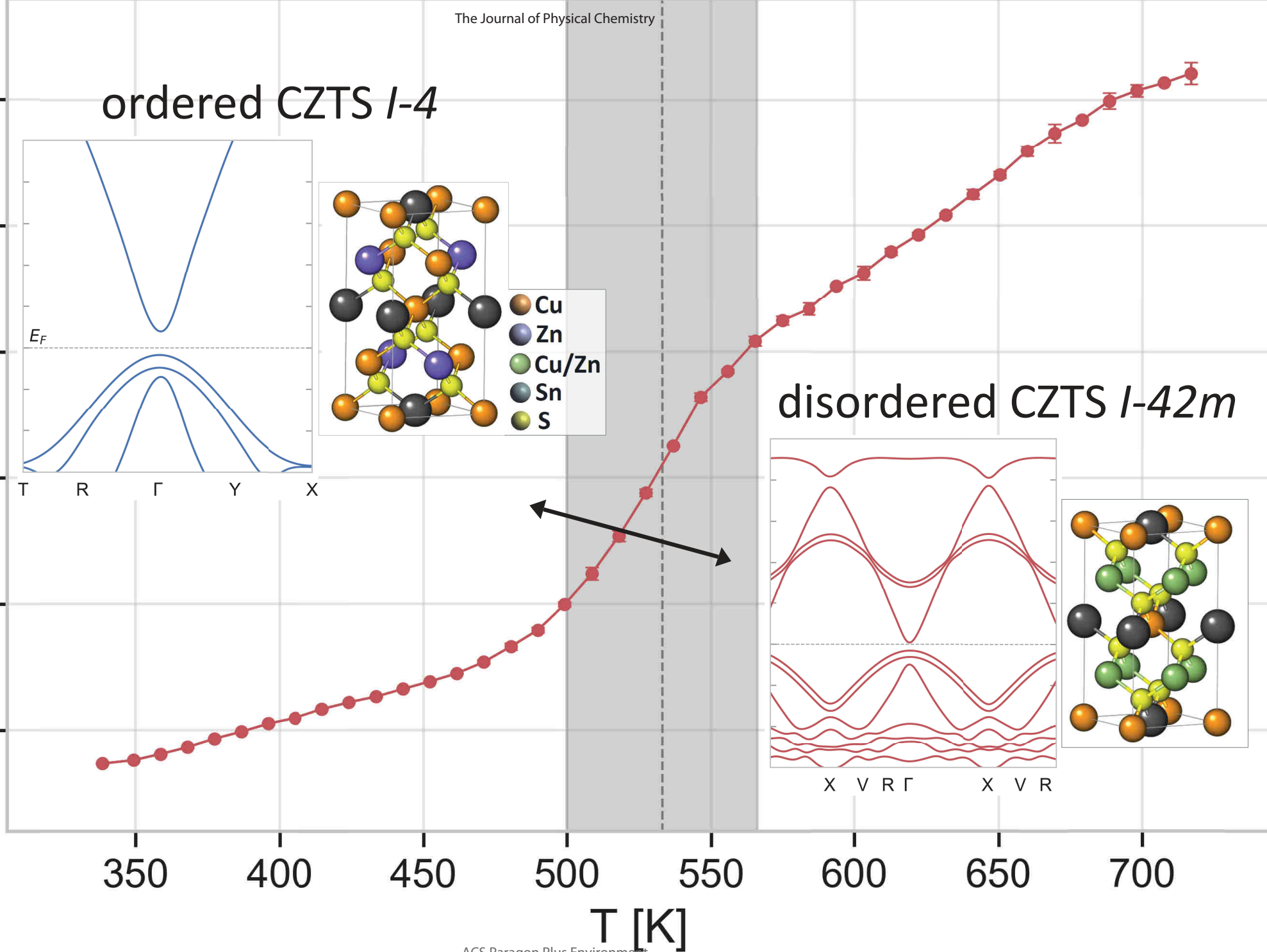
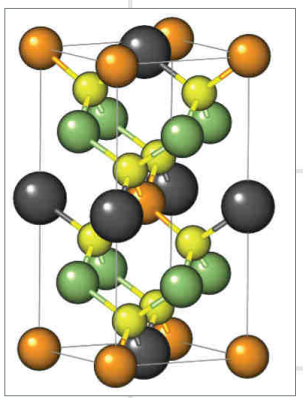
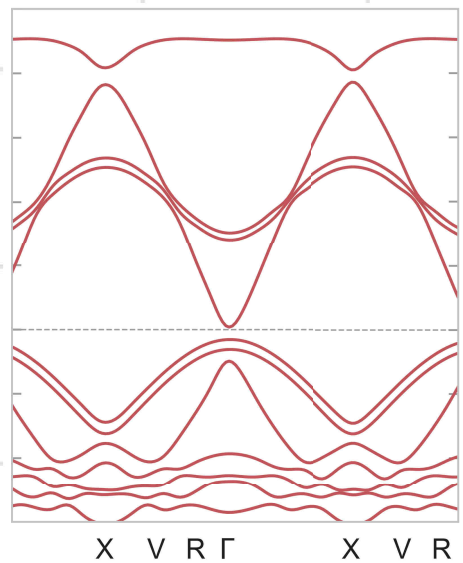
1
2
3
4
5
6
7
8
9
10
11
12
13
14
15
16
17
18
19
20
21
22
23
24
25
26
27
28
29
30
31
32
33
34
35
36
37
38
39
40
41
42
43
44
45
46
47
48
49
50
51
52
53
54
55

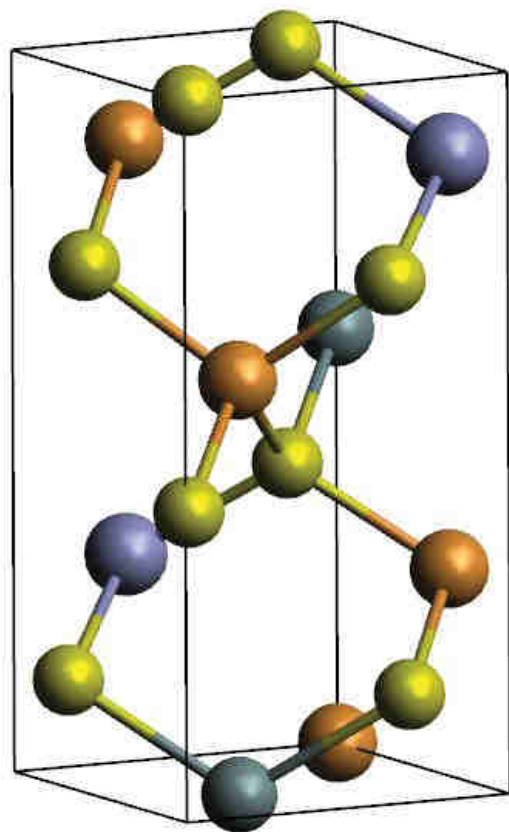
Seebeck coefficient [$\mu\text{V/K}$]

ordered CZTS *I-4*

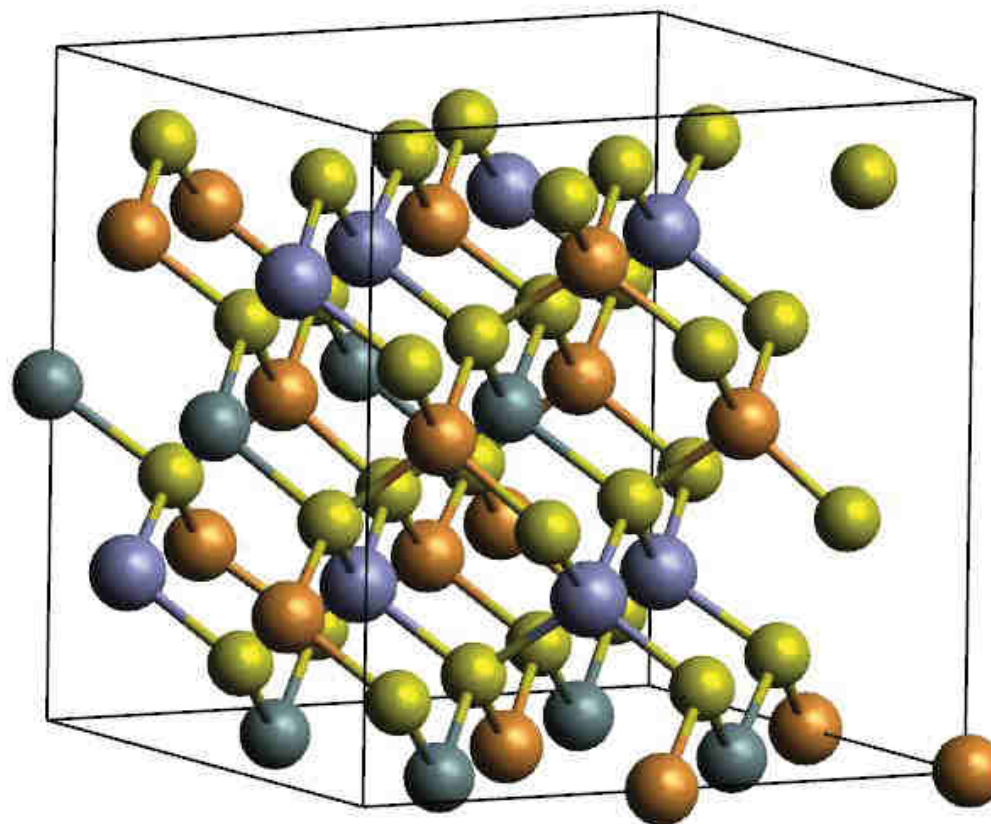


disordered CZTS *I-42m*



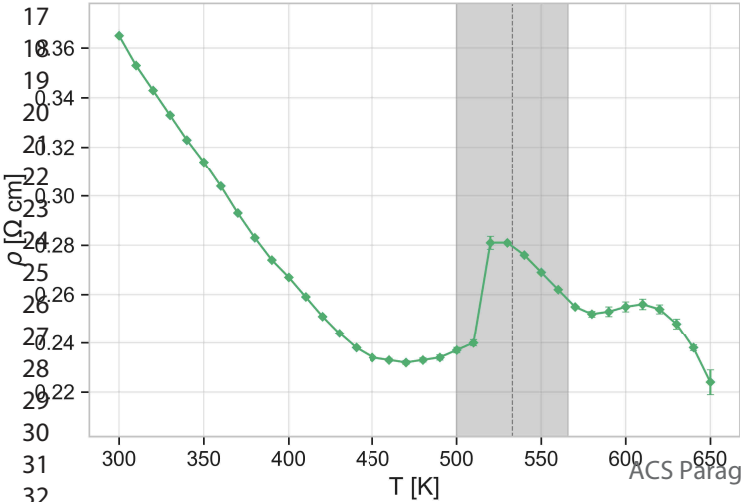
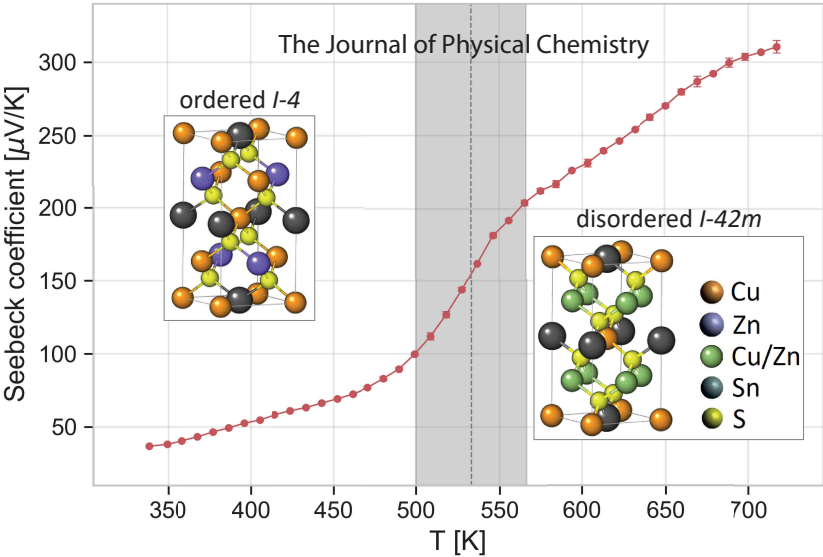


a

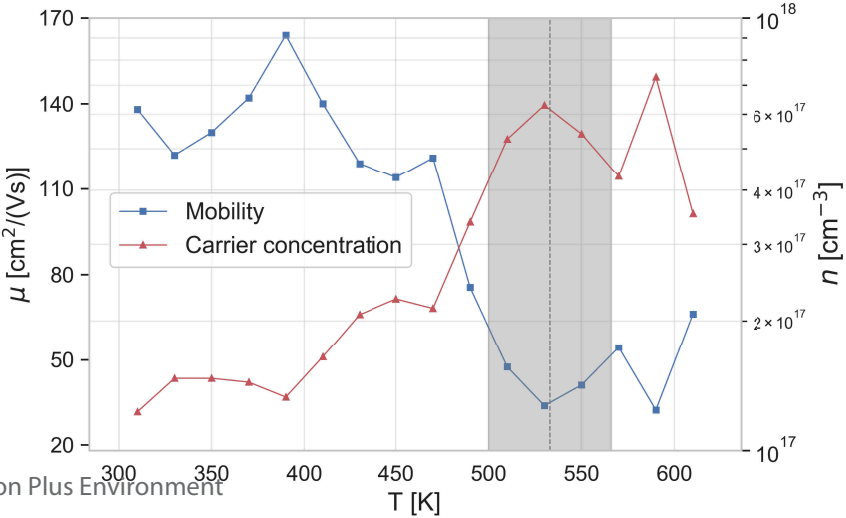


b



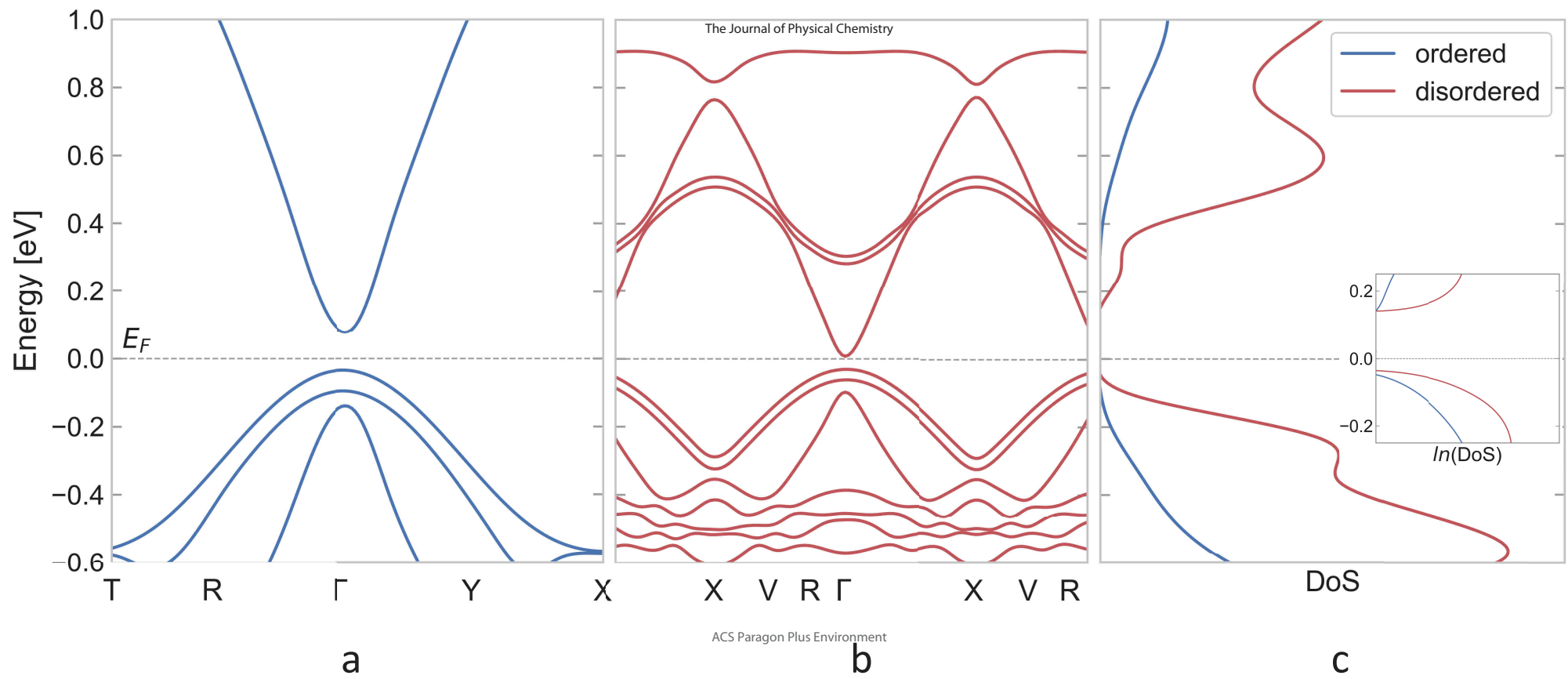


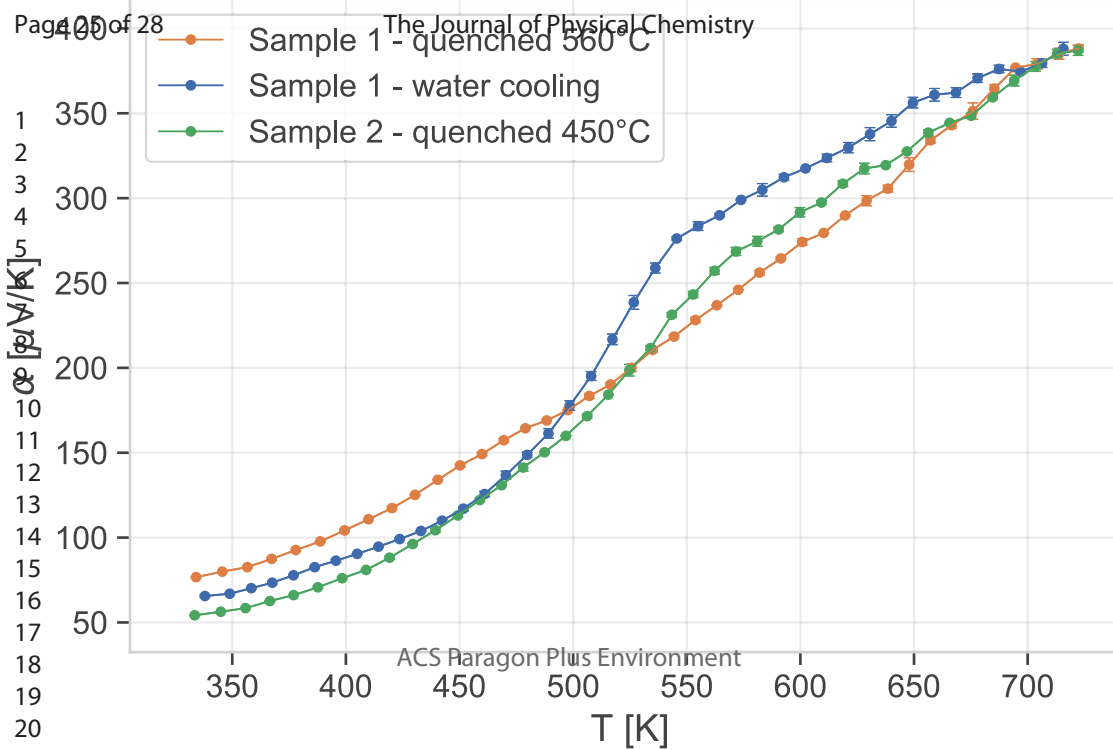
a

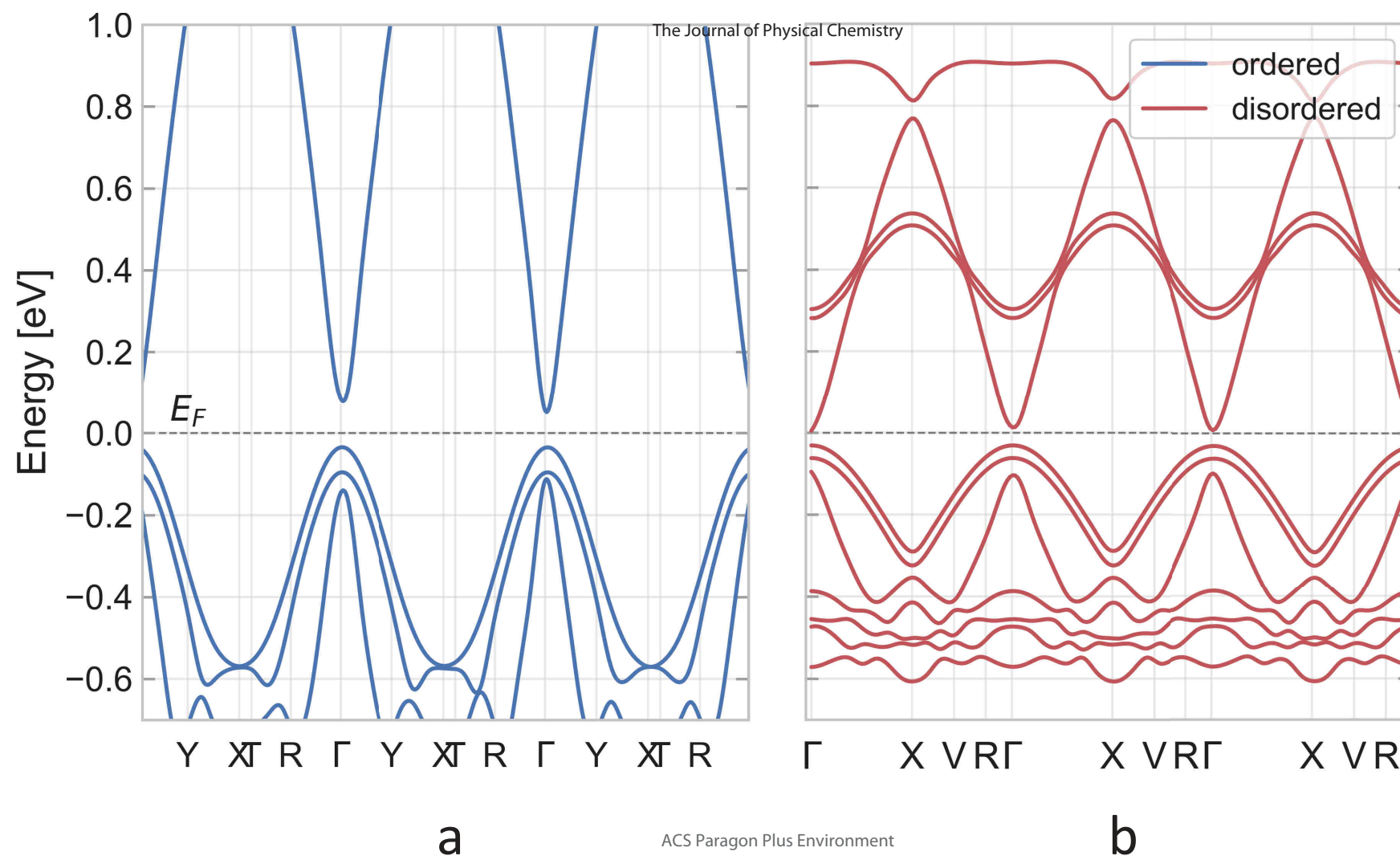


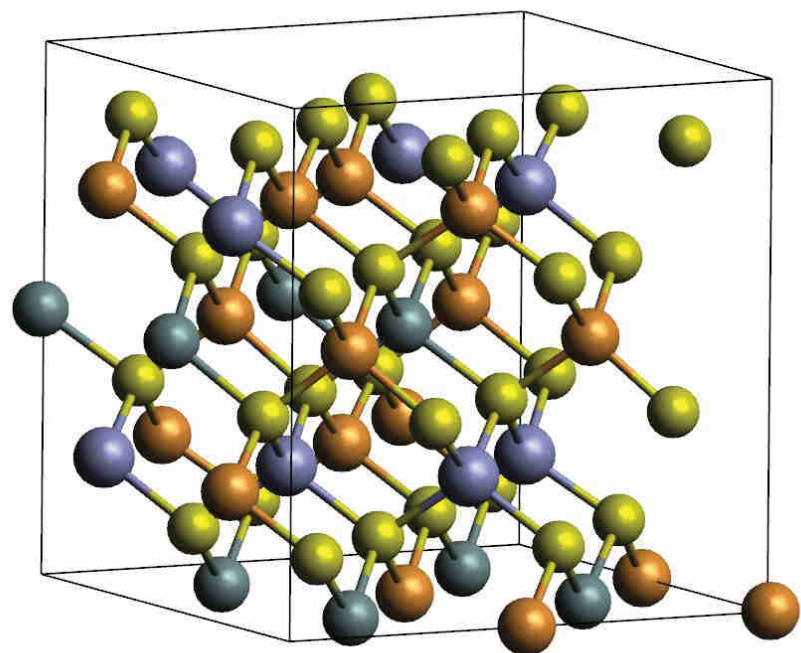
b

c

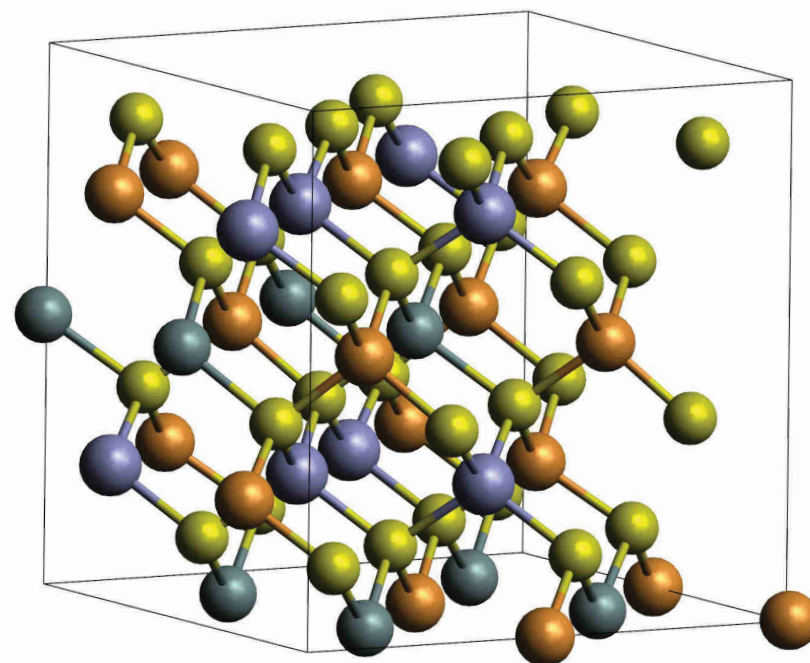








a



b

